Short-term Load Forecasting Using Artificial Neural Network

- Assessment for the 10 Areas in Japan -

Yuji Matsuo*, Kimiya Otani*, Tomofumi Shibata*, Yasuo Yorita*, Yasuaki Kawakami*, Yu Nagatomi*

Abstract

For this paper, we attempted to forecast next-day electricity load in the 10 Japanese areas by using artificial neural networks, a type of artificial intelligence technology. The model used here conducts a principal component analysis of daily load curves and utilizes selective ensembling, indicating good forecasting performance with the mean absolute percentage error limited to less than 2.5%. However, forecasting performances differ widely from season to season, with the percentage error ranging wide from 1.4% in Tohoku to 2.7% in Chugoku and Kyushu. Seasonal changes in errors in Hokkaido and Okinawa differ from those in other regions, reflecting regional characteristics.

As the model used here is a simple one using meteorological data at only one location in each area, more massive data may be used to further improve forecasting performance. Even if forecasting performance is improved in a manner to extend the model, however, summer and winter forecasting errors may still be large. It would be a key future research challenge to consider an advanced forecasting technique assuming abnormal weather conditions and weather forecasting errors.

1. Introduction

Artificial intelligence has evolved remarkably in recent years, attracting interest from not only experts but also a wide range of other people. Attracting attention particularly is the artificial neural network (ANN) technique. This technique has a long history, having been studied in parallel to the evolution of computers since around World War II. As efficient training of multi-layered networks had remained difficult, however, ANN research underwent a series of stagnations called "AI winters" before making great achievements in line with the improvement of the technique, the advancement of computer performance and the expansion of data. Today, multilayer ANN with deep learning techniques sometimes perform even better than humans by learning massive data. In 2017, AlphaGo developed by a subsidiary of Google, which uses a multilayer ANN, defeated the top professional Go player, impressing the world with the effectiveness of the technique. In this paper, we apply the method of ANN to forecast hourly electricity loads over a short term.

Short-term load forecasting (STLF), a key challenge for stable electricity supply, has long been subjected to research. Traditionally, statistical techniques such as the autoregressive moving average (ARMA) model and the autoregressive integrated moving average (ARIMA) model have been used for the STLF. Recently, novel techniques have also been proposed to identify similar days based on past data[1)]. TESLA has reportedly developed a model that combines parameterized non-linear regression model and a time series filter for forecast adjustment[2)]. Electric utilities implement load forecasting for daily operations, trying to accurately forecast load based on meteorological data including temperature, humidity and solar radiation, past similar-day data and interviews with large customers[3) 4)].

While these "traditional" efforts have been continued, machine learning techniques have increasingly been used for load forecasting. Since a review published in 2003 introduced dozens of relevant studies using artificial intelligence[5)], a large number of relevant papers have been published over the last decade. While a number of techniques including support vector machine (SVM) and random forest (RF) have been attempted for STLF, the ANN has recently been subjected to research most frequently. The ANN is widely recognized as improving forecasting performances with advanced techniques, and various techniques have been adopted according to specific objectives. These include not only the expansion of data put into models and the optimization of hyperparameters, but also the utilization of advanced neural networks rather than simple feed-forward ANNs, and their combination with other methods such as genetic algorithms (GA), particle swarm optimization (PSO), gravitational search algorithms (GSA) and adaptive neuro-fuzzy inference systems (ANFIS)[1]. Among the advanced neural networks are recurrent neural networks (RNN), convolutional neural networks (CNN), extreme learning machines (ELM) and radial basis function (RBF) [6)].

* The Institute of Energy Economics, Japan

[1] It must be noted that these are to only a part of the studies seen in the literature published in the past few years.

It is difficult to compare the advantages and disadvantages of these techniques. The first reason for the difficulty is that most studies use only certain data sets for limited regions, days and time zones for assessment. As a matter of course, it is not correct to directly compare documented error figures. Furthermore, any model's forecasting performance widely differs depending on the data set, as explained later. A technique that achieves good forecasting performance for a data set may not necessarily make the same achievement for any other data set. Even for load forecasting for the same region, any technique may not necessarily achieve accurate forecasts for different seasons. Therefore, it is not easy to conclude that any technique is better than any other. Forecasting performances of models based on one technique differ by hyperparameters. In principle, hyperparameters that can produce the best forecasting performance should be selected. Practically, however, as it is excessively time-consuming to optimize all the hyperparameters, they are determined through trial and error in most cases. For this reason, when a researcher compares performances of two models, there is always a risk that the model that he or she wants to recommend is better optimized than the other.

In such situation, trials have also been conducted to compare different models under the same conditions. For example, a group led by Dr. Tao Hong at the University of North Carolina at Charlotte held the Global Energy Forecasting Competition (GEFCom) [7,8] in 2012, 2014 and 2017 for participants to compete in stochastic, deterministic and hierarchical forecasting of electric loads, and solar photovoltaics and wind power generation. The French transmission system operator Réseau de transport d'électricité (RTE) [9] and the Japanese electric utility Tokyo Electric Power Co. (TEPCO)[10] implement their respective competitions in forecasting day-ahead loads.

In this paper, we developed a short-term load forecasting model using the ANN to assess the forecasting performance for each of the 10 Japanese service areas. The model used here, though apparently having high forecasting performance, is a simple one that utilizes meteorological data (weather description and minimum/maximum temperatures) at one location in each area in addition to past electric load and calendar data[2]. Keeping in mind the potential further improvement of the forecasting performance through technical revision and data expansion, we here aimed to assess the forecasting performance for each area and each season, hoping to see further progress in research.

2. Short-term load forecasting (STLF) model using ANN

The ANN is a technique to use massive data for learning a nonlinear relationship between input and output vectors. Its conceptual diagram is given as Figure 2-1.

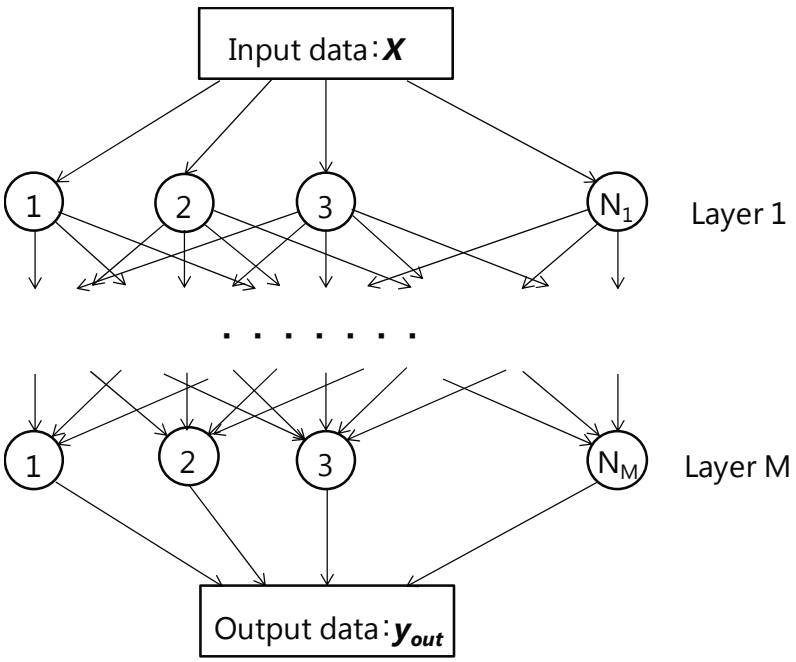

Figure 2-1. A conceptual diagram of the artificial neural network

[2] In contrast, Toshiba Corp.'s model that won the highest award in TEPCO's first electricity load forecasting technology contest is explained as a complex and sophisticated model that uses multipoint AMeDAS data and combines artificial intelligence and sparse modeling technologies.
https://www.toshiba.co.jp/about/press/2017_11/pr_j0801.htm

Here, M "hidden" layers are set between input and output layers. Layer n ($1 \leq n \leq M$) consists of N_n nodes or "neurons." Numerous sets of input vector $\boldsymbol{X}$ and output vector $\boldsymbol{Y}$ are given for training a model before new input data $\boldsymbol{X_F}$ is given to estimate the unknown value of $\boldsymbol{Y_F}$. In general, the more data there are for training, the better the results are. When a future forecast is based on past actual data, however, the data available for training may frequently be limited. As for the electric load forecasting attempted here, for example, load data over a decade may cover only less than 4,000 days, which is not big enough for machine learning. In this case, forecasting performance depends on how efficiently a machine learns from limited data.

In this study, we attempted to forecast hourly electric loads for the next day (Day d+1) at 8 a.m. on Day d, simulating actual operations at an electric utility. Data available for input into a model include calendar data (years, months, days, days of week and national holidays), actual load data until 7 a.m. on Day d, meteorological data (weather description and minimum/maximum temperatures) until Day d-1 and weather forecast data that are made available by the morning of Day d. Although the use of forecast temperature data over 24 hours and forecast humidity data are expected to improve the forecasting performance[11], we used only minimum and maximum temperature data, mainly because of the availability of past forecast data.. Our model analyzes a daily load curve through a principal component analysis (PCA) and adopts selective ensembling to reduce forecasting errors, which enables the model to make significantly better forecasting than a simple ANN. For more details of the model, see Appendix 1.

3. Assumptions and the data used

3-1 Data used for the assessment

3-1-1 Electric load data

In this analysis, we used the ANN for forecasting electric load in the 10 areas, using load data published by the utilities (Table 3-1). We used data between January 1, 2012, and June 30, 2018 for the 9 areas from Hokkaido and Tohoku, and data between April 1, 2016, and June 30, 2018 for Okinawa. These data reflect regional economic activities and weather conditions, as shown in Appendix 2.

Table 3-1 Electric load data used for the study

Area	Period	Number of days	Number of missing data (days)
Hokkaido	Jan. 1, 2012 - Jun 30, 2018	2,341	32
Tohoku	Jan. 1, 2012 - Jun 30, 2018	2,341	32
Tokyo	Jan. 1, 2012 - Jun 30, 2018	2,344	29
Chubu	Jan. 1, 2012 - Jun 30, 2018	2,336	37
Hokuriku	Jan. 1, 2012 - Jun 30, 2018	2,345	28
Kansai	Jan. 1, 2012 - Jun 30, 2018	2,347	26
Chugoku	Jan. 1, 2012 - Jun 30, 2018	2,303	70
Shikoku	Jan. 1, 2012 - Jun 30, 2018	2,372	1
Kyushu	Jan. 1, 2012 - Jun 30, 2018	2,368	0
Okinawa	Apr. 1, 2016 - Jun 30, 2018	820	1

Sources: Websites of former general electric utilities

3-1-2 Meteorological data

As for meteorological data, we used actual data and weather forecasts published by the Japan Meteorological Agency (JMA) for cities where the headquarters of the former general electricity utilities are located (Table 3-2). Specifically, we here used four binary variables, indicating whether the daily weather description includes the words "sunny," "cloudy," "rainy" or "snowy," and maximum/minimum temperatures.

Table 3-2 Areas and representative cities

Area	City	Area	City
Hokkaido	Sapporo	Kansai	Osaka
Tohoku	Sendai	Chugoku	Hiroshima
Tokyo	Tokyo	Shikoku	Takamatsu
Chubu	Nagoya	Kyushu	Fukuoka
Hokuriku	Toyama	Okinawa	Naha

3-2 Modeling framework and evaluation metrics

3-2-1 Modeling framework

In this paper, we used load data given in Table 3-1 for forecasting electric loads between July 2017 and June 2018 and compared forecast and actual data to assess forecasting errors.

When artificial neural networks are used for forecasting, data available at the time of forecasting are usually divided into two parts, one for training and the other for validation. Under the technique given in this paper, we used validation data for selective ensembling.

Here, we adopted a month just before the forecasting period as the validation period. When assessing forecast errors for forecasting in February 2018, for example, we used data between January 2012 (April 2016 for Okinawa) and December 2017 for training and data in January 2018 for validation. Into the model trained with these data, data available in the morning of January 31 were put to forecast load on February 1, then data available in the morning of February 1 were put to forecast load on February 2. We repeated this process to get forecast data through February 28.

The ANNs of the same structure using the same training data may produce different forecasts (and forecasting performances) depending on different initial values, which are given as random numbers. For this paper, therefore, we made 15 computations using different sets of initial values and took the average of the 15 forecast errors to assess the forecasting accuracy of the model.

3-2-2 Evaluation metrics

As performance metrics, we adopted the root mean square error (RMSE) and the mean absolute percentage error (MAPE) defined by the following equations:

$$\mathrm{RMSE} = \sqrt{\frac{1}{n}\sum_{t}(f_t - y_t)^2} \tag{1}$$

$$\mathrm{MAPE} = \frac{1}{n}\sum_{t}\left|\frac{f_t - y_t}{y_t}\right| \tag{2}$$

Here, f_t represents a forecasted load, y_t an actual load, and n the number of data within a forecasting period. As indicated by Equations (1) and (2), the RMSE imposes a greater penalty on a large error than the MAPE, indicating that an RMSE ranking of forecasting performances does not necessarily match a MAPE ranking.

4. Results and discussion

4-1 Short-term load forecasting for the Tokyo area

4-1-1 Examples of forecast results

Figures 4-1, 4-2, 4-3 and 4-4 show forecast and actual data for a summer period (August 21-30, 2017), an autumn period (September 1-10, 2017), a winter period (February 15-24, 2018) and a spring period (April 1-10, 2018), respectively, in Tokyo area. It must be noted that each figure indicates one of 15 projections.

As indicated by these figures, the forecasting error widely differed from season to season even in the same Tokyo

area. The RMSE was as large as 1.95 GW in summer and 1.74 GW in winter and as small as 0.79 GW in autumn and 0.60 GW in spring. For August 28, 2017, in the summer period, for example, the maximum temperature was forecast on the previous day at 28℃ with the weather given as "cloudy," differing far from the actual maximum temperature at 31.4℃ under "cloudy, clear later" weather. As for August 30, the forecast minimum temperature was 27℃, far above the actual one at 24.1℃, though with the forecast maximum temperature at 33℃ close to the actual one. The day's actual weather was rainy, failing to meet the forecast weather.

On February 22, 2018, it snowed against a weather forecast, with the maximum temperature coming at 5.7℃ far below the forecast level of 9℃. On the next day, it was "sleety, temporarily cloudy, clear later" with the maximum temperature at 8.1℃ far below the forecast level of 11℃. In this way, weather forecast error has great influence on load forecasting error. In summer, load generally exceeds the forecast level when the actual temperature is higher than forecast or it is clear against the weather forecast. Conversely, load in winter exceeds the forecast level when the actual temperature is lower than forecast or it is snowy against the weather forecast.

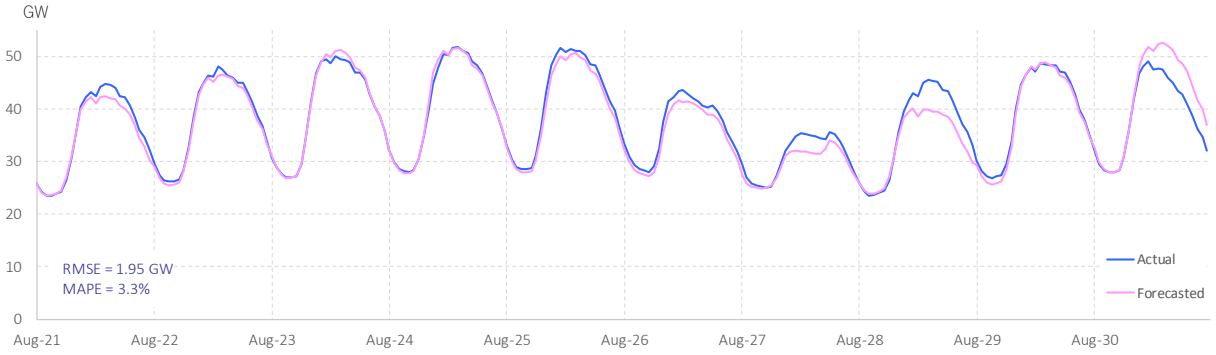

Figure 4-1 Actual and forecasted loads for the Tokyo area (Aug. 21 - 30, 2017)

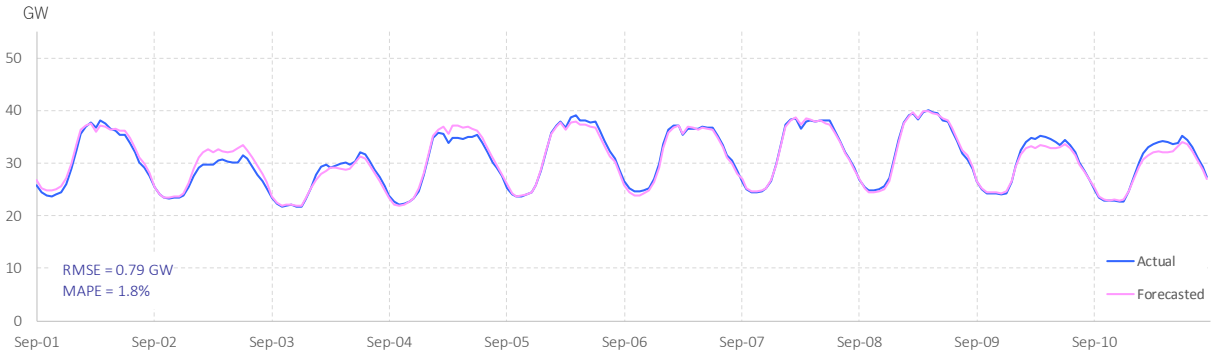

Figure 4-2 Actual and forecasted loads for the Tokyo area (Sep. 1 - 10, 2017)

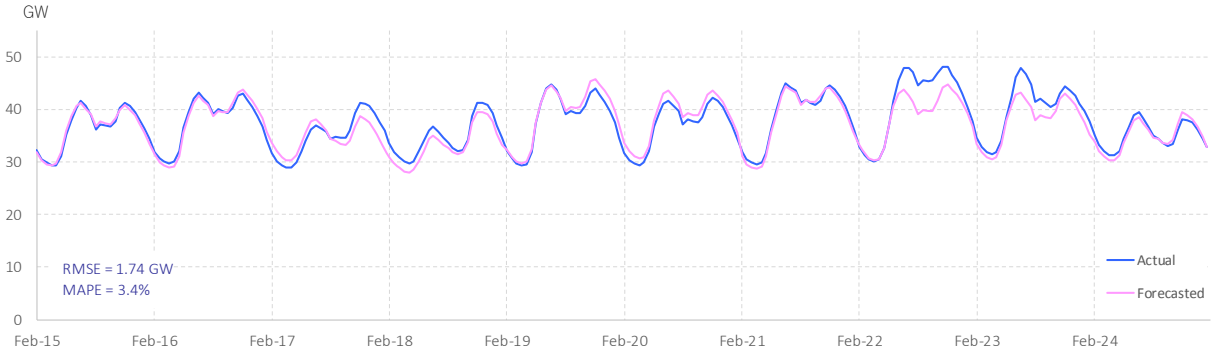

Figure 4-3 Actual and forecasted loads for the Tokyo area (Feb. 15 - 24, 2018)

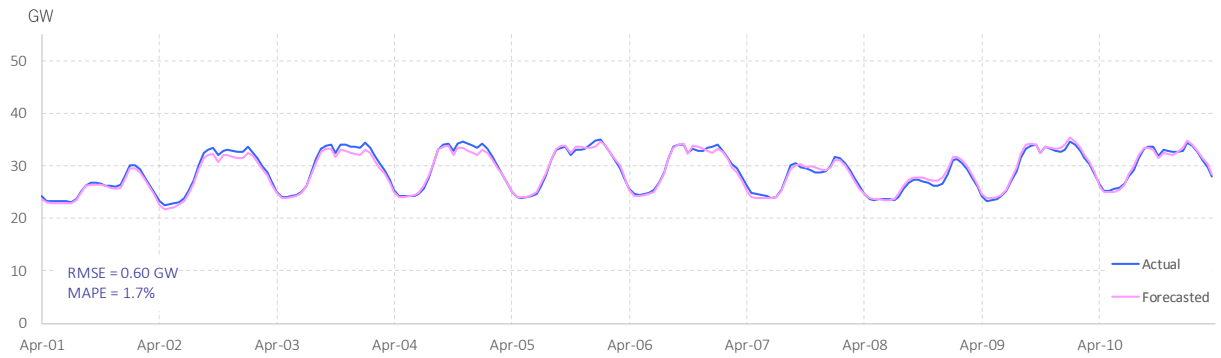

Figure 4-4 Actual and forecasted loads for the Tokyo area (Apr. 1 - 10, 2018)

Of the period given in Figure 4-2, the September 2-10 period matched TEPCO's first electricity load forecasting technology contest period, for which the RMSE came to 0.78 GW. The RMSEs for 15 projections in this period are indicated in a box plot given as Figure 4-5. In a simple case in which no principal component analysis is conducted without selective ensembling, the median and the average for the 15 RMSEs come to 0.86 GW and 0.87 GW, respectively. If selective ensembling is conducted, the median and the average come to 0.83 GW and 0.85 GW, respectively. If a principal component analysis is conducted, they come to 0.81 GW and 0.83 GW, respectively. If both the principal component analysis and selective ensembling are conducted, the median falls further to 0.76 GW and the average declines to 0.78 GW. Given that the RMSE was 0.83 GW for Toshiba that won the highest award in TEPCO's contest, our model was apparently able to achieve good forecasting performance at least for this forecasting period. We should note, however, that forecasting errors largely differ from season to season, meaning that comparison using a small data set may not achieve an appropriate assessment of a model's overall forecasting performance.

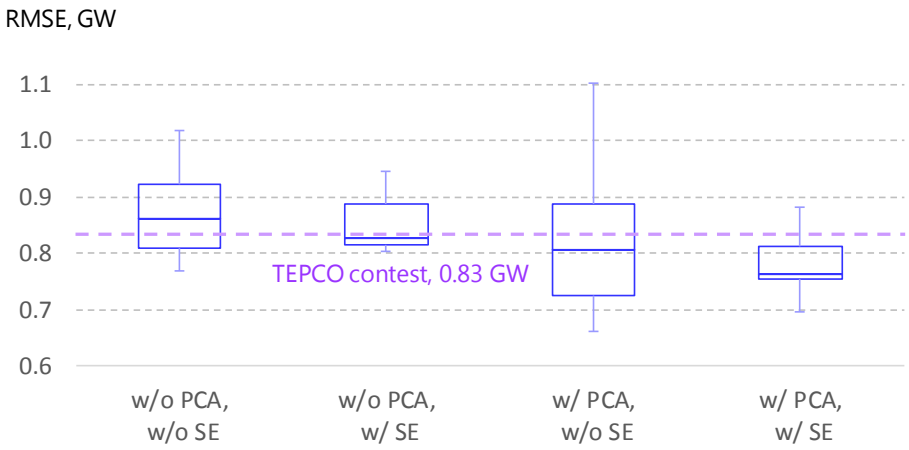

PCA: Principal component analysis, SE: Selective ensembling

Figure 4-5 Forecasting errors for the Tokyo area (RMSE: Sep. 2 – 10, 2017)

4-1-2 Changes in forecasting errors depending on the input data

Changes in forecasting errors depending on the input data are indicated in Figure 4-6 (RMSE) and Figure 4-7 (MAPE). We conducted calculations using the following data:

S: Training with data from April 1, 2016; forecasting using meteorological data at one location (Tokyo)
M: Training with data from January 1, 2012; forecasting using meteorological data at one location (Tokyo)
M2: Training with data from January 1, 2012; forecasting using meteorological data at two locations (Tokyo, Utsunomiya)
MT: Training with data from January 1, 2012; forecasting using meteorological data at one location (Tokyo)
L: Training with data from January 1, 2008; forecasting using meteorological data at one location (Tokyo)

As noted above, forecasts have been made here on 15 different initial conditions, and the average forecasting errors of the 15 forecasts are indicated in Figures 4-6 and 4-7. Noticeably, the RMSE changes with a standard error of around 0.03-0.04 GW, and the MAPE with a standard error of around 0.1% depending on the initial values.

Differences between S, M and L represent gaps between sizes of data sets for training. In general, a model using a larger data set is expected to achieve better forecasting performance. If loads in far and latest past periods indicate different behaviors, however, including far past data may negatively affect forecasting performance. Noticeably, L includes data before the Great East Japan Earthquake and the Fukushima Daiichi nuclear power plant accident in 2011.

Comparison between S and M indicates that M features smaller errors than S in all cases. On an annual average basis, the RMSE is 1.33 GW for S against 1.16 GW for M. The MAPE is 2.7% for S against 2.3% for M. These results indicate that two years of data for training in S is not big enough and that data over a longer period of time for training can improve the forecasting accuracy.

Comparison between M and L indicates that L features smaller errors than M in January and September and greater errors in February and December. On an annual average basis, the RMSE and MAPE for M are almost the same as those for L, showing no statistically significant difference. This means that adding data before 2012 for training fails to improve forecasting performance significantly. However, further consideration must be given to whether the failure is attributable to the power consumption behavior change after the Great East Japan Earthquake or whether it simply means that using data over more than six years cannot improve forecasting performance.

The difference between M and M2 indicate the influence of an increase in the number of locations for the meteorological data. In general, using data at more locations can be expected to reduce forecasting errors. As shown by Figures 4-6 and 4-7, however, M2 has larger errors than M in January, February, March and September but smaller errors in the other months. On an annual average basis, the RMSE is 1.16 GW for M against 1.15 GW for M2. The results do not indicate that the improvement is statistically significant.

MT represents a case in which actual meteorological data are used instead of weather forecast data, which means that this case does not represent "forecasting" results. As a matter of course, errors for MT are far lower than for M. On an annual average basis, the RMSE for MT is 0.9 GW against 1.16 GW for M and the MAPE for MT is 1.9% against 2.3% for M. Even for MT, however, errors in summer and winter tend to be greater than in spring and autumn. This indicates that while weather forecast errors are a major factor behind load forecasting errors, some other factors are behind larger forecasting errors in summer and winter.

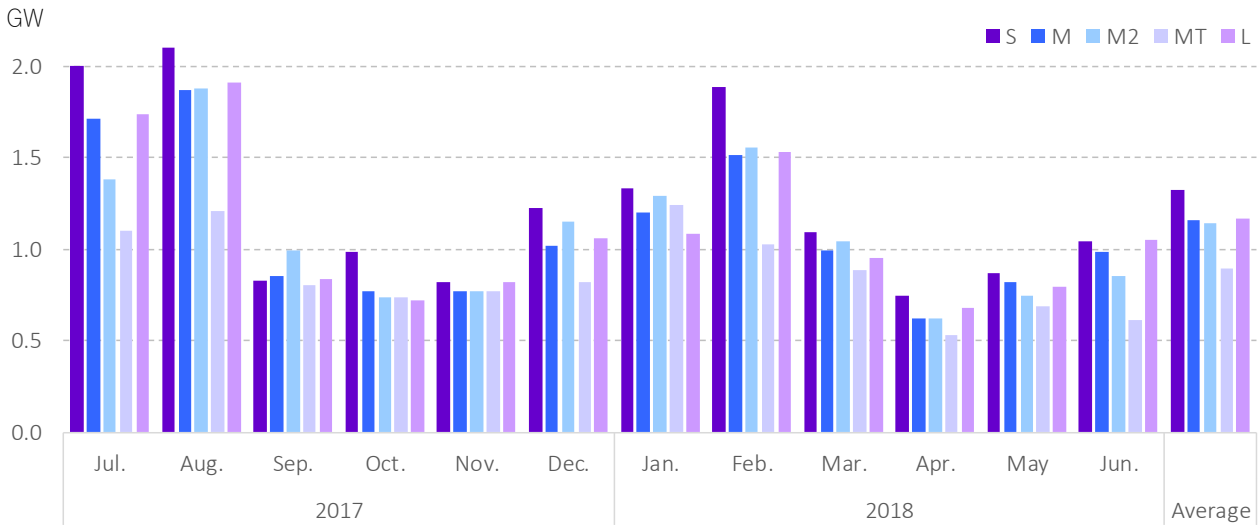

Figure 4-6 Change in forecasting errors (RMSE: Tokyo area)

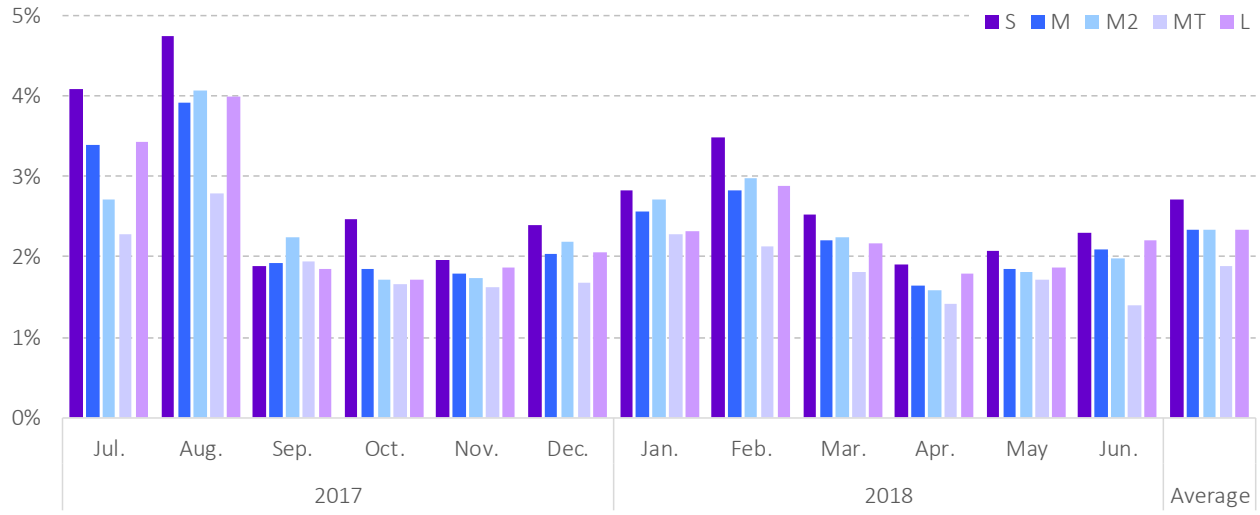

Figure 4-7 Change in forecasting errors (MAPE: Tokyo area)

As indicated by Figures 4-6 and 4-7, the relative scale of forecasting errors between two models, M and M2, changes greatly from month to month. In January 2018, for example, M2 indicates a significantly larger error than M. However, it does not mean that M is a "better" model than M2. In July, for example, M2 indicates a significantly smaller error than M, and on an annual average basis, the two models have no significant gap. This means that it is desirable to use data sets that are as large as possible for comparing different models. At the same time, as far as M and M2 are concerned, it could be said that adding meteorological data at other locations than Tokyo and Utsunomiya, or weighting data for multiple locations with population or electric demand may improve forecasting performance throughout the year.

4-2 Interregional comparison

4-2-1 Examples of forecast results

This section provides forecast results for the June 20-29 period of 2018 in the 10 areas. As noted above, data from 2012 were used for training in all areas other than Okinawa, and data from 2016 were used for Okinawa. Meteorological data at one location of each area were used for training and forecasting.

(1) Hokkaido

In the Hokkaido area, the average load in the June 20-29 period stood at 3.07 GW, with the maximum load at 3.62 GW recorded at 4 p.m. on June 29 (Friday) and the minimum at 2.58 GW at midnight on June 26 (Tuesday). As load fluctuated in a narrow range of about 1 GW in the period, it was supposed to be relatively easy to forecast load. The average RMSE came to a favorable level of 0.07 GW. On June 23 (Saturday) when the actual maximum temperature came to 26.2℃, 11.2℃ above the forecast level of 15℃, however, the RMSE stood at 0.095 GW with the MAPE at 2.4%, indicating worse forecasting accuracy than on the other days. Particularly between 10 a.m. and 5 p.m. when actual temperatures apparently deviated far from forecast levels, the RMSE stood at 0.15 GW indicating an underestimated forecast for a long time. At 11 a.m. on June 26 (Tuesday), a forecast indicated the largest deviation from an actual level. The maximum load at that time was 3.45 GW, about 0.23 GW more than the forecast level. This was because the unexpected load peak in the morning failed to be forecast. Similarly, forecasts deviated from actual levels on June 20 (Wednesday), 22 (Friday) and 27 (Wednesday), but on each of these days, the forecast maximum and minimum temperatures deviated little from the actual levels. If these exceptional peaks in the morning were triggered by temperature changes, forecasting accuracy may be improved by using 24 hourly temperature forecast data, rather than the maximum and minimum temperatures.

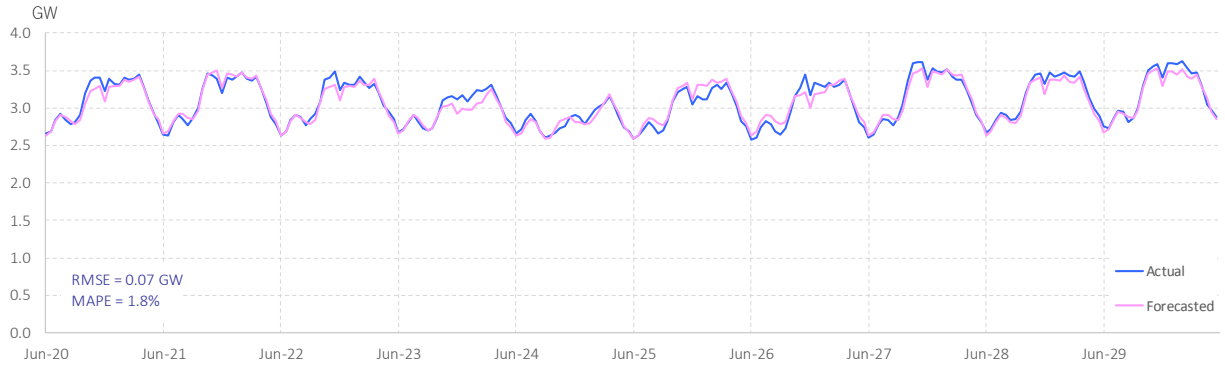

Figure 4-8　Actual and forecasted loads: Hokkaido area

(2) Tohoku

In the Tohoku area, the average load in the June 20-29 period stood at 6.82 GW, with the maximum load at 8.1 GW recorded at 11 a.m. on June 29 (Friday) and the minimum at 5.94 GW at 1 a.m. on June 24 (Sunday). Load fluctuated in a relatively narrow range of 2 GW in the period. The average RMSE came to a favorable level of 0.13 GW, with the MAPE standing at 1.3%. The average MAPE indicated the highest accuracy among the 10 areas for the period. On June 26 (Tuesday) and 29 (Friday), the RMSE stood at 0.18 GW and 0.25 GW, with the MAPE at 2.1% and 2.7%, indicating that forecast levels deviated relatively largely from actual levels on these days. It can be said that on these two days, temperature changes in Sendai differed much from those in other locations, such as Niigata, which were not used for training the model. On June 26, for example, the maximum temperature fell by 4℃ from the previous day in Sendai while rising by 7.6℃ in Niigata. These underestimated forecasts on these two days came apparently as forecasting failed to cover load increases in other locations. As the Tohoku area is large and encompasses cities with different climate conditions, using meteorological data at only one location may fail to indicate load changes in other locations.

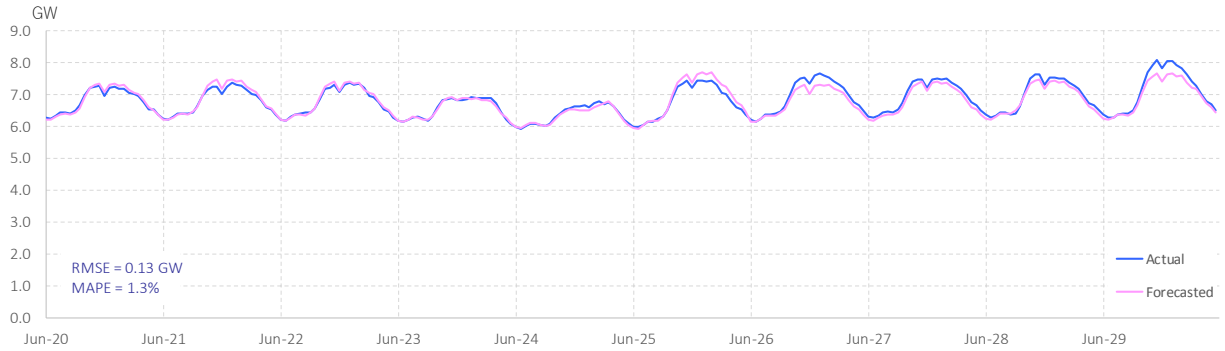

Figure 4-9　Actual and forecasted loads: Tohoku area

(3) Tokyo

In the Tokyo area, the average load in the June 20-29 period stood at 33.16 GW, with the maximum load at 47.27 GW recorded at 2 p.m. on June 29 (Friday) and the minimum at 22.13 GW at 5 a.m. on June 24 (Sunday). The RMSE stood at 0.81 GW, indicating the model's good forecasting performance. On June 27 (Wednesday), however, the model forecast the maximum load at 42.57 GW slipping far below the actual level of 45.40 GW. The maximum and minimum temperatures on the day came to 31.7℃ and 24.9℃, deviating from the forecast levels of 30.0℃ and 23.0℃. This implies that the forecast load errors on these days are due mainly to the forecast weather errors.

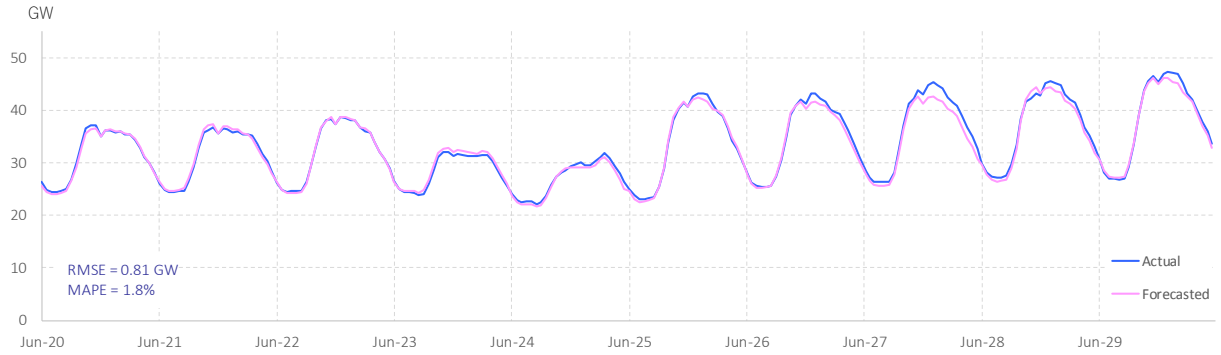

Figure 4-10　Actual and forecasted loads: Tokyo area

(4) Chubu

In the Chubu area, the average load in the June 20-29 period stood at 15.78 GW, with the maximum load at 21.30 GW recorded at 2 p.m. on June 28 (Thursday) and the minimum at 9.97 GW at 6 a.m. on June 24 (Sunday). While the RMSE stood at 0.45 GW indicating generally good forecasting performance, forecast load levels slipped far below actual levels in the afternoons of Jun 25 (Monday), 26 (Tuesday) and 27 (Wednesday) (the average deviation came to 0.67 GW, with the maximum one at 1.24 GW). On the three days, the actual maximum temperatures were an average 1.5℃ higher than the forecast levels. Although the actual maximum temperature was 2.5℃ higher than the forecast level on June 27, the three-day average deviation was not more remarkable than the average for other days in the forecasting period.

Meanwhile, the actual maximum temperature remained at or below 30.0℃ until June 23 (Saturday) before rising to 31.1℃ on June 24 (Sunday) and 33.9℃ on June 25 (Monday) rewriting a year-to-date high for the second straight day. Given this temperature trend, forecasting errors during this period are supposed to have expanded due to the increase in air cooling demand along with the rapid temperature rises.

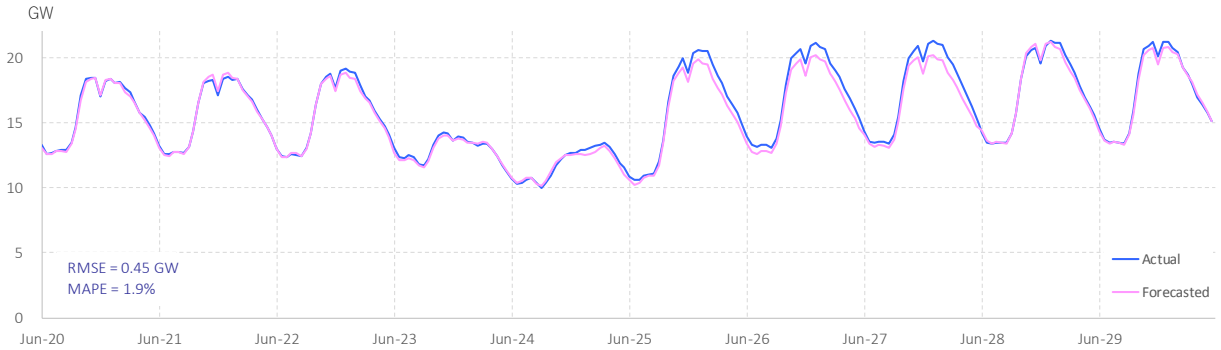

Figure 4-11　Actual and forecasted loads: Chubu area

(5) Hokuriku

In the Hokuriku area, the average load in the June 20-29 period stood at 3.33 GW, with the maximum load at 4.40 GW recorded at 11 a.m. on June 29 (Friday) and the minimum at 2.32 GW at 7 a.m. on June 24 (Sunday). While the RMSE stood at 0.12 GW indicating good forecasting performance, forecast load levels were far higher than actual levels in the afternoon of June 29 (Friday). At 4 p.m. on the day, the actual load stood at 4.01 GW, far below the forecast level of 4.51 GW, indicating the largest overestimate in the period. The day's actual maximum temperature stood at 30.7℃ against the forecast level of 34.0℃, indicating that a weather forecast error led to a large load forecast error.

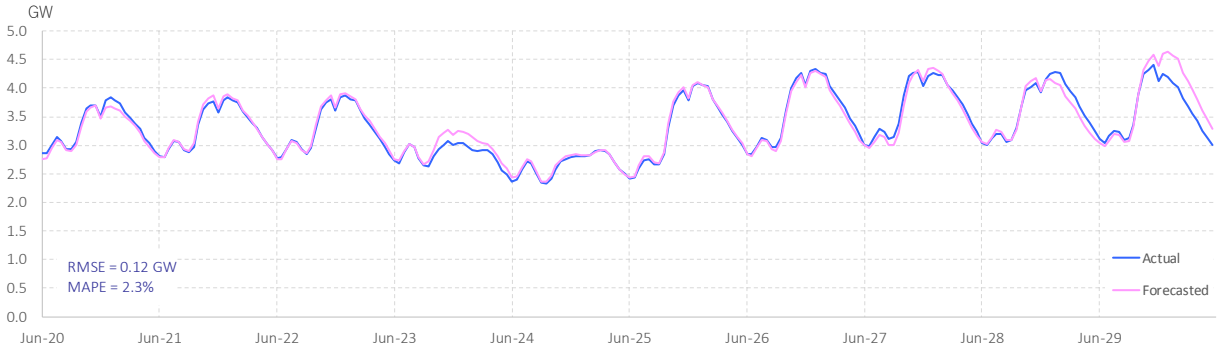

Figure 4-12　Actual and forecasted loads: Hokuriku area

(6) Kansai

In the Kansai area, the average load in the June 20-29 period stood at 16.81 GW, with the maximum load at 23.19 GW recorded at 2 p.m. on June 28 (Thursday) and the minimum at 1.16 GW at 1 a.m. on June 24 (Sunday). The RMSE stood at 0.70 GW with the MAPE at 3.0%, indicating slightly worse forecasting accuracy than in other regions. Particularly between 9 a.m. and 6 p.m. on June 25 (Monday), 26 (Tuesday) and 27 (Wednesday), forecast load levels were far lower than actual levels.

A factor behind the large deviation for the three days may be that actual maximum temperatures were an average 2.1℃ higher than forecast levels. Furthermore, the daily maximum temperature remained at or below 30.0℃ until June 24 (Sunday) before rising to 33.1℃ on June 25 (Monday) rewriting a year-to-date high and standing at 31.6℃ on June 26 (Tuesday) and at 33.5℃ on June 27 (Thursday), suggesting that the model failed to accurately forecast a rapid increase in air cooling demand.

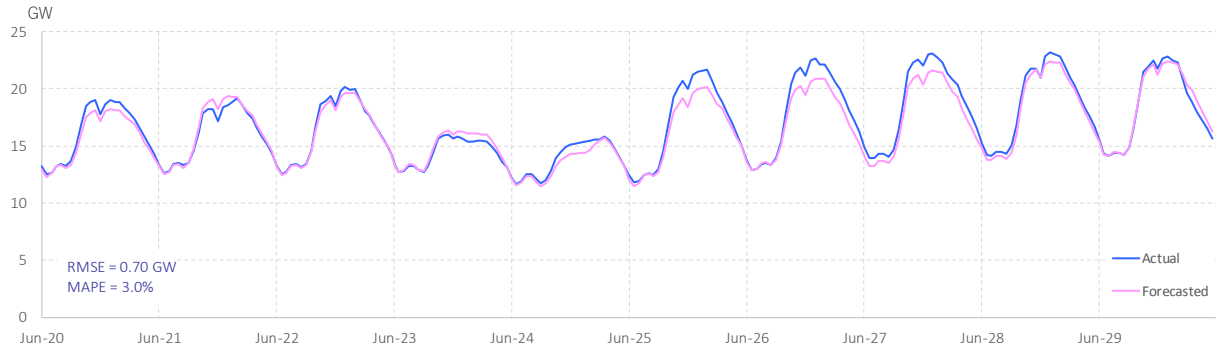

Figure 4-13　Actual and forecasted loads: Kansai area

(7) Chugoku

In the Chugoku area, the average load in the June 20-29 period stood at 6.79 GW, with the maximum load at 8.76 GW recorded at 2 p.m. on June 28 (Thursday) and the minimum at 5.06 GW at 1 a.m. on June 24 (Sunday). Maximum load levels were more than forecast levels for six days from June 24 (Sunday) to 29 (Friday), leading the MAPE to stand at 2.8% representing the eighth highest accuracy among the 10 areas. The relatively large error may be attributable to wild fluctuations in daily maximum temperatures and forecast temperatures' deviation from actual levels. The daily maximum temperature rose by as much as 4.0℃ from the previous day to 31.1℃ on June 25 (Monday), the highest for the calendar day since 2012, before falling by as much as 5.0℃ to 26.1℃ on June 26 (Tuesday). The actual maximum temperature was 2.9℃ higher than forecast on June 26 (Tuesday) and 2.7℃ lower on June 28 (Thursday). The actual minimum temperature was 2.2℃ lower than forecast on June 24 (Sunday) and 2.4℃ higher on June 29 (Friday).

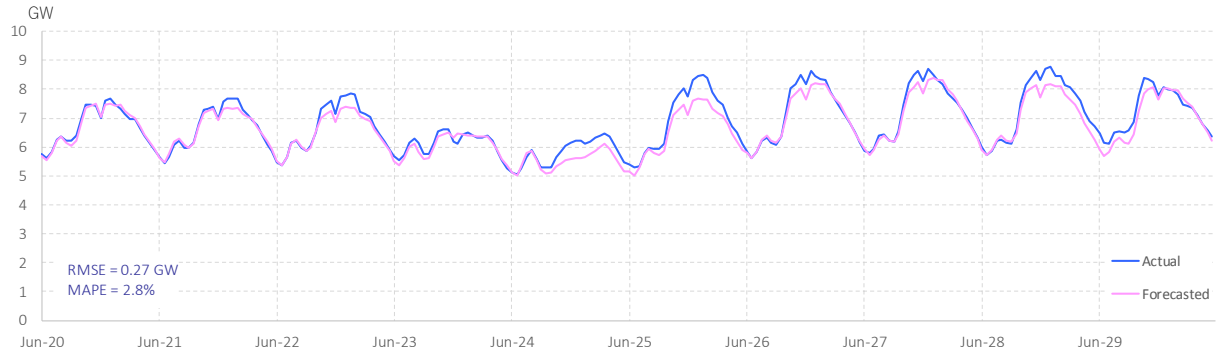

Figure 4-14　Actual and forecasted loads: Chugoku area

(8) Shikoku

In the Shikoku area, the average load in the June 20-29 period stood at 3.13 GW, with the maximum load at 4.26 GW recorded at 2 p.m. on June 28 (Thursday) and the minimum at 2.23 GW at 7 a.m. on June 24 (Sunday). The forecast load was lower than the actual on June 20 (Wednesday), 25 (Monday), 26 (Tuesday) and 27 (Wednesday). On June 20 (Wednesday), the maximum temperature came to 23.7℃ against the forecast level of 25℃, indicating that a weather forecast error led to a large load forecast error. On June 25 (Monday), 26 (Tuesday) and 27 (Wednesday), maximum temperature levels were 3-5℃ higher than the 2012-2017 averages for these days, suggesting that cooling demand emerged earlier than normal, leading to load forecast errors.

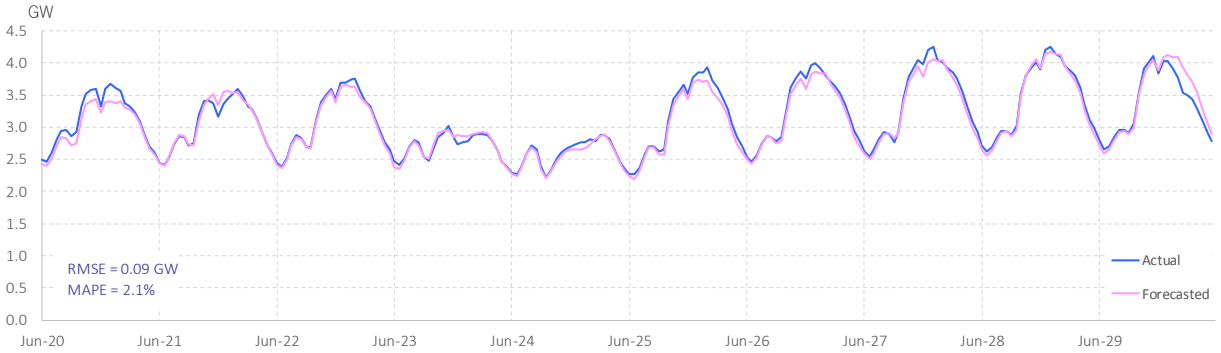

Figure 4-15　Actual and forecasted loads: Shikoku area

(9) Kyushu

In the Kyushu area, the average load in the June 20-29 period stood at 9.97 GW, with the maximum load at 12.73 GW recorded at 1 p.m. on June 27 (Wednesday) and the minimum at 7.19 GW at 1 a.m. on June 24 (Sunday). Actual load levels deviated far from forecast levels for five days from June 22 (Friday) to June 26 (Tuesday), leading the MAPE to stand at 3.6%, the worst among the 10 areas. On June 23 (Saturday), the actual maximum temperature came to 24.5℃, 6.5℃ lower than the forecast level of 31℃, resulting in an overestimated load forecast. On June 22 (Friday), 23 (Saturday), 25 (Monday) and 26 (Tuesday), rain came despite no-rain forecasts, suggesting that unstable weather conditions contributed to worsening the forecasting accuracy.

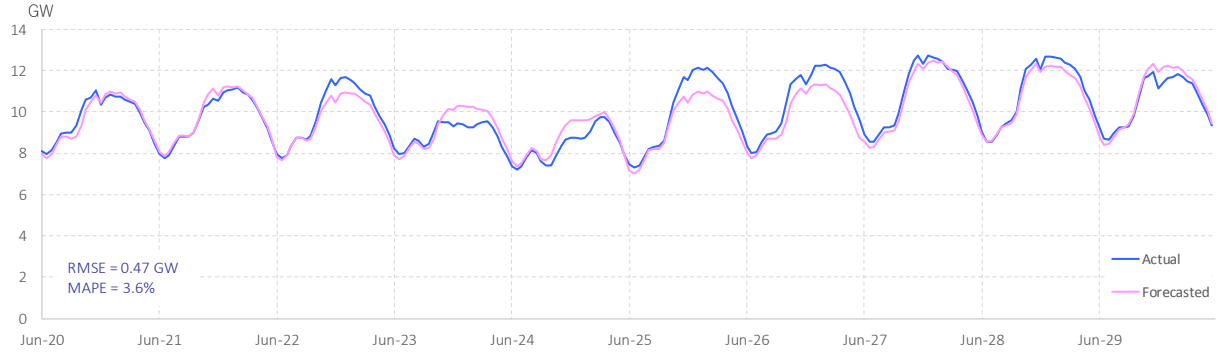

Figure 4-16　Actual and forecasted loads: Kyushu area

(10) Okinawa

In the Okinawa area, the average load in the June 20-29 period stood at 1.16 GW, with the maximum load at 1.41 GW recorded at 3 p.m. on June 28 (Thursday) and the minimum at 0.88 GW at 3 a.m. on June 23 (Saturday). In this area that features an annual average MAPE at 3.0%, the largest among the 10 areas, as explained later, the period's MAPE was limited to a relatively good level of 1.7%. This may be because daily load curves are similar or stable in the period. However, the forecast load was slightly less than the actual on June 24 (Sunday) and slightly more on June 25 (Monday). Nevertheless, the maximum and minimum temperatures' deviations from forecast levels were limited to less than 1℃ on the two days. Although meteorological data in Naha alone were used for forecasting load this time, in Okinawa that comprises a large number of small islands, an interesting challenge is to explore how using data at more locations could improve the load forecasting performance.

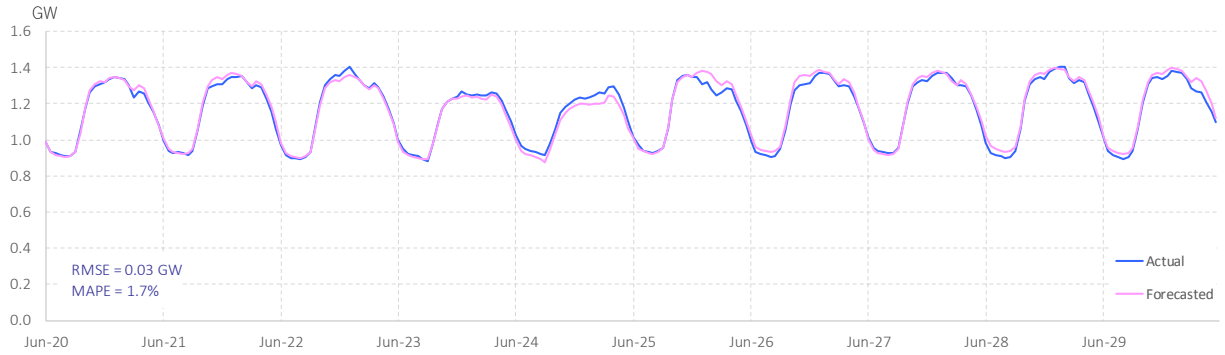

Figure 4-17 Actual and forecasted loads: Okinawa area

4-2-2 Changes in monthly forecasting errors

Monthly load forecasting errors (MAPE) in the 10 areas are given in Table 4-1 and Figure 4-18. As indicated here, in most of the areas, MAPE is larger in summer (July and August) and winter (January and February). Among the areas, Tohoku features a remarkably small MAPE of 1.4% against relatively larger MAPE in Chugoku, Kyushu and Okinawa. The larger MAPE for Okinawa may be partly explained by the limited range of data for training. As suggested by Figure 4-19, MAPE is larger during daytime and smaller during nighttime. Noticeably, daily error curves in Hokkaido and Okinawa differ significantly from those in other areas.

Hokkaido, Hokuriku, Kansai and Kyushu Electric Power Companies provide past forecast load data in their respective service areas on their respective websites. For the period between July 2017 and June 2018, the MAPE stood at about 3.1%, 2.4%, 2.5% and 2.4%, respectively. Given that their forecasts were made at different time points, these MAPE levels cannot be compared directly with each other. Furthermore, attention must be paid to the fact that electric utilities tend to set load forecasts at higher levels from the viewpoint of stable electricity supply[12]. Given that our forecasts for this paper are made in the morning on Day *d* or earlier than electric utilities' forecasts and based on a limited range of input data, however, the average MAPE just below 2.5% given in Table 4-1 can be interpreted as indicating fairly good forecasting performance.

Table 4-1　Forecasting errors by area and month (MAPE)

	2017						2018						Average
	Jul.	Aug.	Sep.	Oct.	Nov.	Dec.	Jan.	Feb.	Mar.	Apr.	May	Jun.	
Hokkaido	2.8%	2.1%	2.3%	2.2%	2.4%	2.5%	2.5%	2.3%	3.0%	2.6%	2.1%	1.8%	2.4%
Tohoku	2.0%	1.8%	1.4%	1.0%	1.2%	1.5%	1.6%	1.9%	1.7%	1.1%	0.9%	1.2%	1.4%
Tokyo	3.4%	3.9%	1.9%	1.9%	1.8%	2.0%	2.6%	2.8%	2.2%	1.6%	1.8%	2.1%	2.3%
Chubu	2.2%	3.8%	2.6%	2.2%	1.7%	2.2%	2.9%	1.9%	2.0%	2.0%	2.1%	1.6%	2.3%
Hokuriku	3.0%	3.0%	2.1%	1.6%	2.5%	2.7%	3.0%	2.9%	2.6%	2.0%	2.2%	2.2%	2.5%
Kansai	2.6%	3.7%	2.4%	2.3%	1.9%	1.9%	2.5%	2.4%	2.1%	1.8%	1.7%	2.3%	2.3%
Chugoku	3.3%	3.9%	3.0%	2.3%	2.3%	2.5%	3.0%	2.5%	2.6%	2.2%	2.8%	2.4%	2.7%
Shikoku	3.0%	3.0%	2.6%	2.3%	2.0%	2.7%	3.1%	2.8%	2.5%	2.0%	1.9%	1.9%	2.5%
Kyushu	2.7%	3.8%	3.3%	2.6%	2.0%	2.5%	3.1%	2.9%	2.6%	2.4%	2.0%	2.7%	2.7%
Okinawa	2.3%	2.4%	3.8%	3.9%	2.7%	2.3%	2.8%	3.6%	2.4%	2.6%	3.6%	3.2%	3.0%

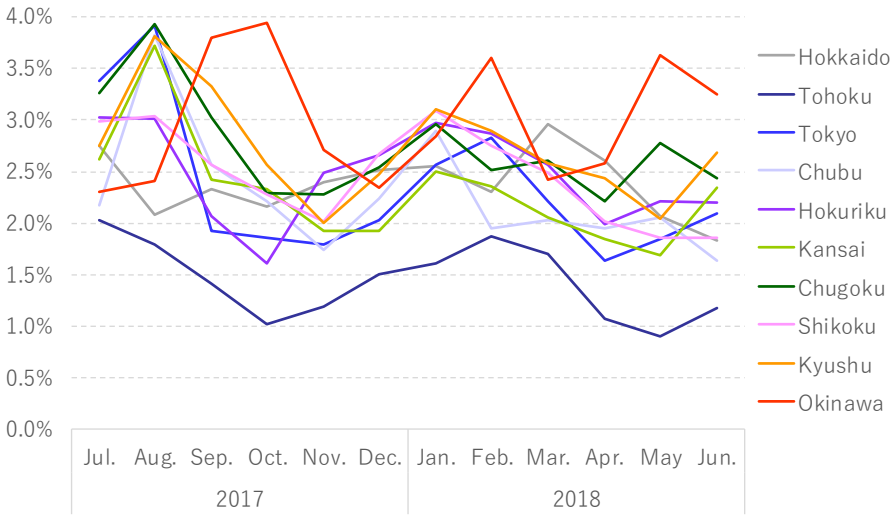

Figure 4-18　Forecasted errors by area and month (MAPE)

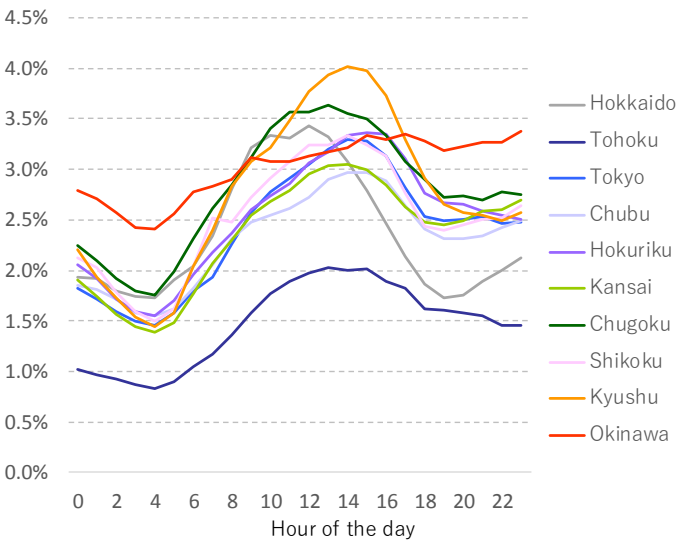

Figure 4-19　Forecasted errors by area and hour of the day (MAPE)

Figure 4-20 indicates the distribution of regional percentage forecasting errors (the absolute differences between forecast and actual data divided by actual data). The graph gives a forecasting percentage error for 131,400 data (365 days × 24 hours × 15 computations) rounded to one decimal place for each area, representing a relative frequency of the percentage errors.

The distribution is wider in Okinawa and narrower in Tohoku. In most of the regions, forecasting error rates remain within a range between -5% and +5%.

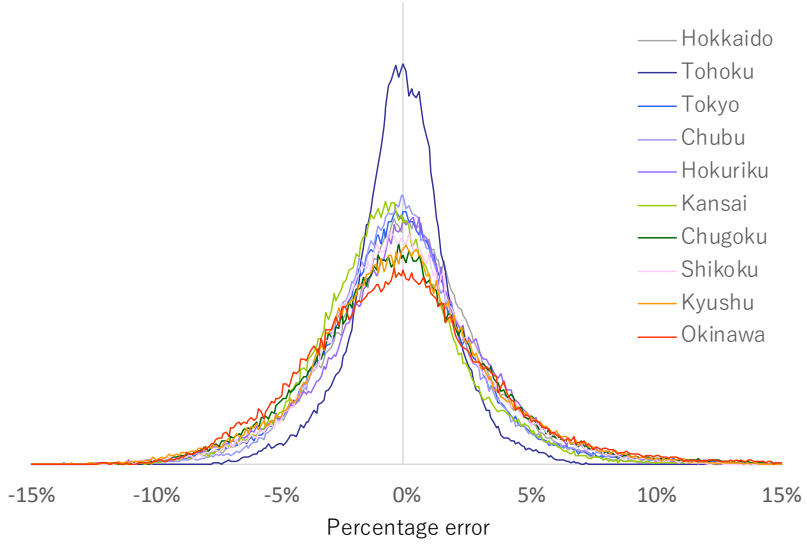

Figure 4-20　Distribution of percentage errors by area

Worthy of attention is the fact that load fluctuations are wilder in summer and winter that feature greater forecasting errors. Figure 4-21, which locates each month's standard deviation of load divided by the annual average load on the abscissa and each month's average MAPE on the ordinate, indicates their correlation. Given the correlation, the smaller forecasting error in Tohoku may partly be explained by the fact that load fluctuations in the area are smaller than in other areas (see Appendix 2). Unlike other areas, Hokkaido features larger errors in March than in January or February. This may be related to the region's standard deviation of load in March that is larger than in January or February.

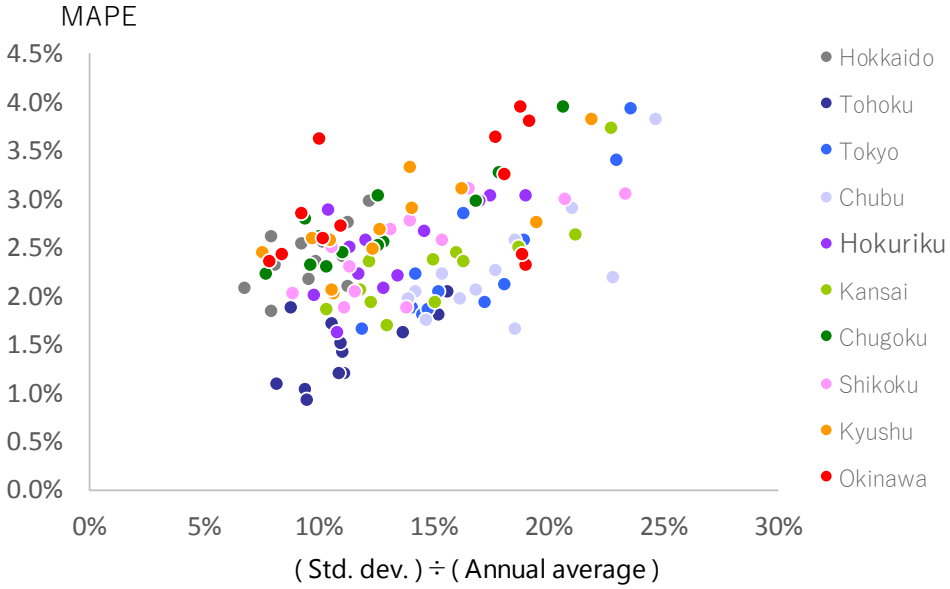

Figure 4-21　Correlation between MAPE and the standard deviation of electric load

5. Conclusion

For this paper, we attempted to forecast short-term load for the 10 areas in Japan by using an artificial neural network utilizing meteorological data at one location of each region. The load forecasting task here was divided into three steps, and selective ensembling was conducted at each step for accurate forecasting. Forecasting errors were larger for summer and winter featuring wilder load fluctuations and smaller for spring and autumn. Errors were smaller for Tohoku and larger for Chugoku and Kyushu. Months seeing larger errors in Hokkaido and Okinawa differed from those in other regions, indicating regional characteristics.

The ANN model used here may have potential to further improve its forecasting performance by expanding input data to include humidity and forecast hourly temperature data, by utilizing meteorological data at more locations and by increasing the number of selective ensembling. As indicated by this paper, however, a model that indicates good forecasting performance on a specific data set does not necessarily perform well constantly. This suggests that careful consideration is required for comparing merits of forecasting models and that as much data as possible should be utilized for assessment. Given that some models are suitable for some seasons and unsuitable for others, a forecasting model using an ANN with the techniques described in this paper may be combined with other techniques to further improve the forecasting performance. Meanwhile, selective ensembling is effective for improving the forecasting performance and may be applicable for other forecasting tasks.

At the same time, even if the model is significantly improved with more advanced techniques, forecasting errors in summer and winter may still be large. Although the number of days seeing large forecasting errors is limited, with most of such errors being attributable to weather forecast errors[3], the results of this paper suggests that weather forecast errors are not the only factor behind load forecasting errors. Exploring factors behind errors to further improve the forecasting performance is one of the key future research challenges.

References

1) M. Tucci et al., 2016. A multi-objective method for short-term load forecasting in European countries. *IEEE Trans. Power Syst.*, 31(5), pp. 3537-3547.
2) TESLA, Inc. "Our Method." http://www.teslaforecast.com/about-tesla/our-method/
3) Ministry of Economy, Trade and Industry, 2017. "Document Presented by the Secretariat for the 25th Meeting of Institutional Design Experts" http://www.emsc.meti.go.jp/activity/emsc_system/pdf/025_05_00.pdf
4) Y. Matsubara, 2018. "Service Area Load Forecasting System and Forecasting Solar Photovoltaics Output," *Energy & Resources* 39(1), pp.50-54.
5) K. Metaxiotis et al., 2003. Artificial intelligence in short term electric load forecasting: a state-of-the-art survey for the researcher. *Energy Convers. Manag.*, 44(9), pp. 1525-1534.
6) F. M. Bianchi et al., 2017. *Recurrent Neural Networks for Short-Term Load Forecasting: An Overview and Comparative Analysis.* Springer. ISBN: 978-3319703374.
7) T. Hong et al., 2014. Global energy forecasting competition 2012. *Int. J. Forecasting*, 30(2), pp. 357-363.
8) T. Hong et al., 2016. Probabilistic energy forecasting: Global Energy Forecasting Competition 2014 and beyond. *Int. J. Forecasting*, 32(3), pp. 896-913.
9) Réseau de transport d'électricité, 2018. Prévision déterministe de la consommation électrique hivernale (volet 1). https://www.datascience.net/fr/challenge/33/details
10) Tokyo Electric Power Company Holdings, Inc. 2017 "'1st Load Forecasting Competition' to Compete for Accurate Load Forecasting" http://www.tepco.co.jp/press/news/2017/1440911_8963.html
11) R. Salkuti. (2018). Short-term electrical load forecasting using radial basis function neural networks considering weather factors. *Electr. Eng.* pp.1-11. https://doi.org/10.1007/s00202-018-0678-8
12) Hokkaido Electric Power Co., 2017. "Future Load Forecasting Technique" http://www.emsc.meti.go.jp/activity/emsc_system/pdf/025_05_01.pdf
13) D. P. Kingma and J. Ba, 2014. Adam: A method for stochastic optimization. https://arxiv.org/abs/1412.6980
14) Y. Matsuo and T. Oyama, 2018. Forecasting daily electricity demand by applying artificial neural network with Fourier transform and principal component analysis techniques. The 13th International Symposium on Operations Research and its Applications, Session 5-3.
15) Y. Matsuo and T. Oyama, 2018. Short-term electric demand forecasting using artificial neural networks with daily load curve analysis techniques. Operational Research Society of Japan, Autumn 2018 Forum on Research Works, 2-E-9.
16) Z.-H. Zhou et al., 2002. Ensembling neural networks: Many could be better than all. *Artif. Intell.*, 137, pp. 239-263.

[3] Past data lead us to estimate that weather forecast errors are not random but regular to some extent. Explicit consideration to such regularity is likely to improve the forecasting performance to some extent.

Appendix 1 Load forecasting model using principal component analysis (PCA) and selective ensembling

Appendix 1-1 Artificial Neural Network (ANN)

In general, the ANN comprises input and output layers and one or multiple median layers, as indicated by Figure 2-1. If the input data are expressed as an N_0-dimensional vector $\boldsymbol{y_0} = \boldsymbol{X}$, and the n-th hidden layer as an N_0-dimensional vector $\boldsymbol{y_n}$, we can sequentially calculate output data $\boldsymbol{y_{out}} = \boldsymbol{y_{M+1}}$ from input data $\boldsymbol{X}$ by the following equation:

$$\boldsymbol{y_{n+1}} = f(\boldsymbol{w_n y_n} + \boldsymbol{b_n}) \qquad n \in \{0, 1, \ldots, M\} \tag{A1}$$

Here, f represents a nonlinear function called an activation function. Matrix $\boldsymbol{w_n}$ and vector $\boldsymbol{b_n}$ are parameters called weights and biases, respectively. The nonlinear nature of the activation function allows complex systems to be modelized for highly accurate forecasting.

Massive sets of input data $\boldsymbol{X}$ and output data (or "teacher" data) $\boldsymbol{Y}$ are prepared as data for the training of the neural network. Then, $\boldsymbol{w_n}$ and $\boldsymbol{b_n}$ are optimized to minimize the difference between the output and the teacher data (in most cases, a square Euclidean distance between $\boldsymbol{y_{out}}$ and $\boldsymbol{Y}$ is adopted as the difference). In general, a gradient descent method is here used to solve this optimization problem, and various variations of gradient descent methods have been proposed to efficiently find the optimal point. The gradient descent method first sets the initial $\boldsymbol{w_n}$ and $\boldsymbol{b_n}$ values randomly and descends the gradient to find optimum $\boldsymbol{w_n}$ and $\boldsymbol{b_n}$ values. Here, attention must be paid to the point that results differ depending on the initial values. The number of hidden layers M and the number of each layer's neurons N_i are hyperparameters to define the model. Because there is no established method to set these parameters, they must be set through trial and error. The model for this paper used the softplus function defined as $f(x) = \log(1 + e^x)$ as the activation function, and set M and N_i at 3 and 30, respectively. We used Adam[13] as the gradient descent method.

Appendix 1-2 Principal component analysis to analyze daily load curves

The principal component analysis (PCA) is a method widely used to extract major features from massive data. Given here is a data set having m variables $x_1, x_2, \ldots, x_m$ (i.e., n set of m-dimensional data $\boldsymbol{X_1}, \boldsymbol{X_2}, \ldots, \boldsymbol{X_n}$, $\boldsymbol{X_k} = [x_1^{(k)}, x_2^{(k)}, \ldots, x_m^{(k)}]$ and $k \in [1, 2, \ldots, n]$). Define a linear combination z_1 of these variables as follows:

$$z_1 = w_{11}x_1 + w_{21}x_2 + \cdots + w_{m1}x_m \tag{A2}$$

When the coefficients w_{i1} ($i = 1, 2, \ldots, m$) are determined to maximize the variance of z_1 on condition of $w_{11}^2 + w_{21}^2 + \ldots + w_{m1}^2 = 1$, z_1 is called the first principal component (PC). In the same way, if the coefficients of the linear combination $z_2 = w_{12}x_1 + w_{22}x_2 + \ldots + w_{m2}x_m$ are determined to maximize the variance of z_2 under the condition $w_{12}^2 + w_{22}^2 + \ldots + w_{m2}^2 = 1$ in the m-1-dimensional space orthogonal to z_1, z_2 is called the second PC. If this procedure is iterated to prepare up to the i-th PC ($i < m$) and the data set is approximated by these PCs precisely enough, the m-dimensional data set will have been successfully reduced into an i-dimensional space. Mathematically, PCs can be determined as the eigenvector of the covariance matrix.

Hourly electric load on a day can be considered a vector in a 24-dimensional space ($m = 24$). For example, load curves in the Tokyo area were subjected to PCA to illustrate 1st to 4th PCs (PC1-4) as shown on Figure A-1, allowing a load curve on a specific day to be approximated as a linear combination of these PCs, and the coefficients of the linear combination are called principal component scores (PC scores). In the model used for this paper, the four PC scores for each of all past days were calculated for learning to forecast the four PC scores for the next day. This dimension reduction can significantly improve the forecasting performance[14, 15].

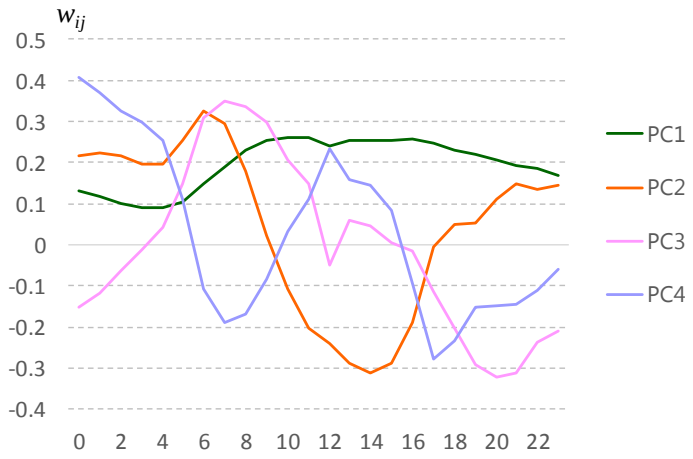

Figure A-1 Principal components (Tokyo area)

In the field of machine learning, it is known that an autoencoder can be used for dimension reduction to further generalize the PCA method. Therefore, the autoencoder may have been used instead of PCA to develop a model that would achieve the same or better forecasting performance. As far as an electric load analysis is concerned, however, the cumulative proportion of the four PCs shown in Figure A-1 exceeds 99%, allowing PCA to enable a considerably accurate approximation. For this reason, we used the PCA method for the model.

Appendix 1-3 Selective ensembling

It is widely recognized that when machine learning is used for forecasting, adopting the ensemble average of results from multiple models rather than results from a single model can improve the forecasting performance. Taking advantage of this, many studies have attempted more advanced "ensemble learning" (such as bugging or boosting) methods in which multiple models are efficiently trained for more accurate forecasting.

In contrast, Zhou et al. (2002)[16] indicated that "selective ensembling" could improve the forecasting or classifying performance. Instead of simply averaging results from multiple models for making forecasts, the selective ensembling method assessed model output errors for the validation data before forecasting, excluded models producing large errors and used the remaining models for taking an ensemble average. Zhou et al. used the genetic algorithm to select models to be excluded.

The approach we used for this paper sets the validation data on which the output errors are significantly correlated to forecasting errors, and then selects the models used for forecasting. It could be called the "empirical selective ensembling" method. Assume a school class of 40 students. While the Zhou et al. approach excludes several dull students and adopts the average of the remaining students' answer as the final one, our approach adopts the average of answers only from several smart students, preparing beforehand the standards which can efficiently decide whether any specific student is smart or dull.

Our approach is based on the following observation regarding the STLF. If the validation data are randomly selected among the training data as done for many machine learning models, no significant correlation is seen between errors in the validation and the test (forecasting) data. If the data for the latest several days right before the test data are adopted as the validation data, however, significant correlations are seen between the errors for the validation and the test data. The contrast may be attributable to a gap between periods for training and forecasting for the STLF. The forecasting targets of STLF are day-ahead loads, while the training period extends to several years. Although training the model with data over a longer past period results in higher forecasting performance in general, it may also be well expected that load data three years ago may not be as useful as those three days ago for forecasting tomorrow data.

Our procedure is given below: When load in January 2018 are used as test data for assessing the forecasting performance, data for the latest n_V days (if n_V is 10, data for December 22-31, 2017) are adopted as the validation data and earlier data (until December 21, 2017) as the training data. The training data are used to train models from n_T sets of initial conditions and the errors on the validation data are assessed using the n_T models obtained. Then, n_S ($1 \leqq n_S \leqq n_T$) models with the smallest errors are selected, where n_S is determined to minimize average output errors on the validation data. Finally, the mathematical average of forecast values of the n_S models is adopted as the final forecast.

As indicated by the name "empirical selective ensembling," n_V is set empirically. While a smaller n_V may destabilize assessment, a too-high n_V value may cover data on days having little correlation with test data and reduce the effect of the selection. Here, we set n_V at 30. As a matter of course, if the n_T value is larger (if excellent students are selected from all 200 students of the same grade rather than from 40 students in a class), the forecasting performance may be better, which we can confirm by numerical experiments. This represents a tradeoff with a longer computation time. For this paper, we set n_T at 20.

Appendix 1-4 Structure of the STLF model

This paper represents assessment using a short-term load forecasting model that utilizes PCA and selective ensembling. Here, the following data are adopted as input data for the model to forecast 24-hour load data on Day *d*+1 at 8 a.m. on Day *d*:

Electric load data: Day *d*-1 (24-hour data), Day *d* (until 7 a.m.)
Calendar data (year, month, day, day of week, national holiday): Days *d*-1, *d*, *d*+1, *d*+2
Meteorological data (maximum temperature, minimum temperature, weather description): Day *d*-1
Weather forecast data (maximum temperature, minimum temperature, weather description): Days *d*-1, *d*, *d*+1

Natural numbers of the calendar data (years, months and days) and the maximum and minimum temperatures in degrees Celsius are used as they are. Among the days of week, Sunday is set as 0, Monday as 1, Tuesday as 2, Wednesday as 3, Thursday as 4, Friday as 5 and Saturday as 6. National holidays, December 29-31, January 1-3 and August 13-16 are set as 1 and the other days as 0. As for weather description, four binary variables representing sunny (or clear) (W_1), rainy (W_2), cloudy (W_3) and snowy (W_4) days are prepared. If the weather description published by the Japan Meteorological Agency (JMA) includes any of these words, each of the variables is set as 1, and 0 otherwise. For example, if a day's weather description is "clear, occasionally cloudy, temporarily snowy, with snowstorm," the variables are given as W_1=W_3=W_4=1 and W_2=0. For the weather forecast data, we used those obtained in the morning on the previous day. All values are standardized according to the following equation:

$$x_t = \frac{X_t - \bar{X}}{X_{max} - X_{min}} \tag{A3}$$

Here, X_t stands for the original value. $\bar{X}$, X_{max} and X_{min} are the mean, maximum and minimum values of X_t, respectively.

The model is outlined by Figure A-2.

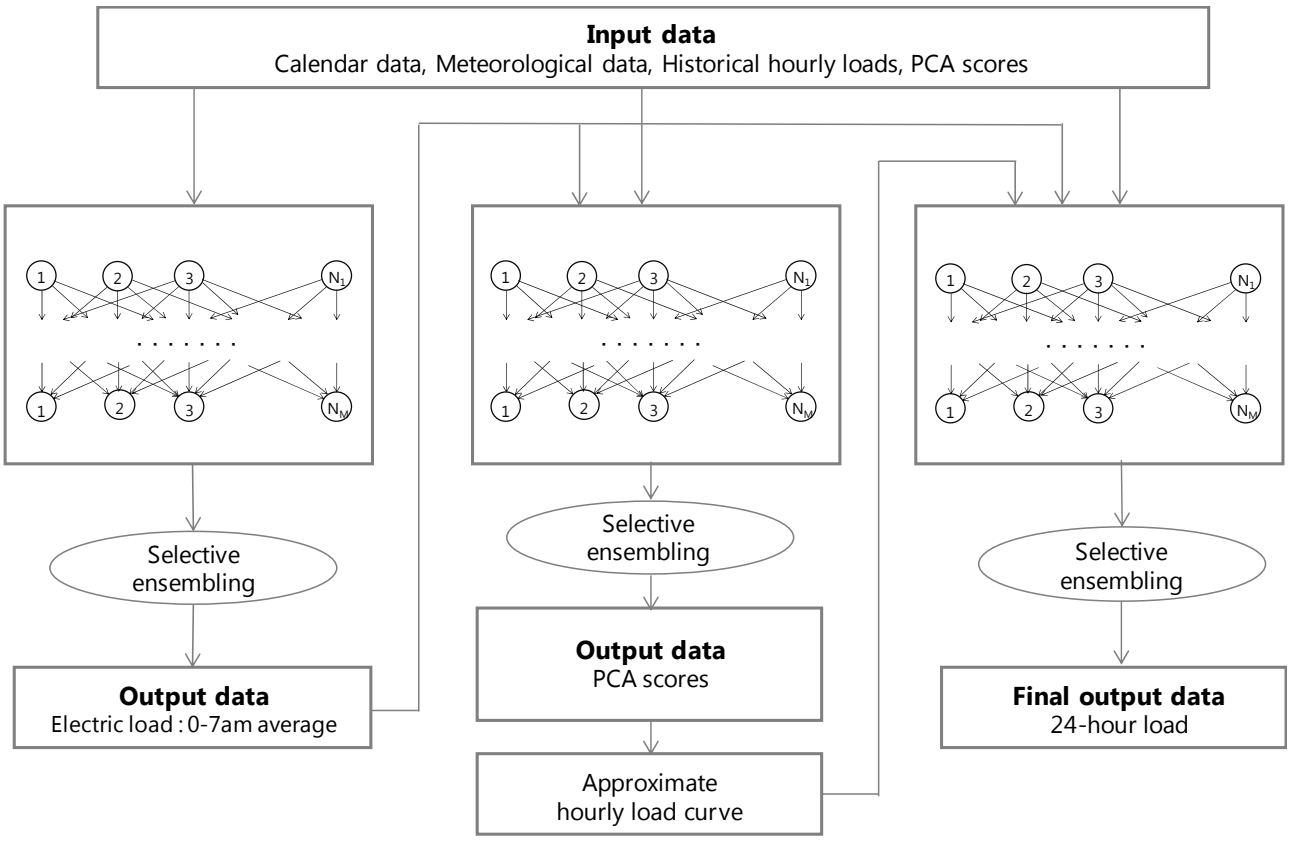

Figure A-2 Short-term load forecasting model using PCA and selective ensembling

As indicated here, the forecasting task is divided into three steps. In the first step, the model forecasts the average load between 0 a.m. and 7 a.m. on Day d+1, given as $h_{7,d+1}$. In the second step, $h_{7,d+1}$ is added to input data, with the 1st to 4th PC scores until Day d-1 adopted as input data, to forecast PC scores for Day d+1. After obtaining an approximate load curve for Day d+1 from the forecast PC scores, we added the curve to input data in the third step to forecast 24-hour load data for Day d+1. In each step, the selective ensembling method was applied with n_T at 20. On average, forecast load data tended to slip slightly below actual data in a biased manner. So, we assessed the 24 hourly average forecasting error for 30 days before the day, and subtracted the values from final output hourly loads. This adjustment allowed the MAPE to fall by 0.1 percentage points on average for most of the areas.

In addition to PCA, there are other various methods to analyze load curves, including the discrete Fourier transform, k-means and fuzzy c-means. More simply, daily, morning and afternoon average load data may be adopted as input data, instead of PC scores, to forecast 24-hour data. Among the methods we tried, the discrete Fourier transform method and a method using morning and afternoon averages produced forecasting results that are as excellent as or slightly worse than those from PCA, while the fuzzy c-means method produced only worse results. It is not easy, however, to compare merits of models. The assessment of modelling techniques suitable for different seasons and different load curve shapes is left as an interesting challenge for the future.

Appendix 2 Average daily load curves by area

Figure A-3 indicates spring (March-May), summer (June-August), autumn (September-November), winter (December-February) and annual average daily load curves in each area during April 1, 2017, and March 31, 2018. In most of the areas, load is larger in summer and winter and smaller in spring and autumn. It is smaller in summer in Hokkaido and in winter in Okinawa, indicating regional differences. Load in spring is smaller than in autumn. This may be partly explained by hysteretic human practices to use air conditioners differently even at the same temperatures.

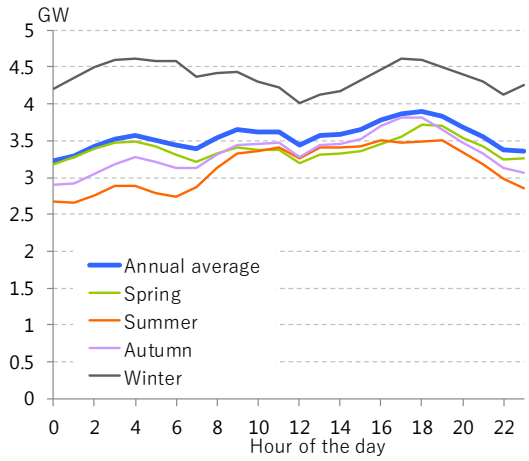

Hokkaido

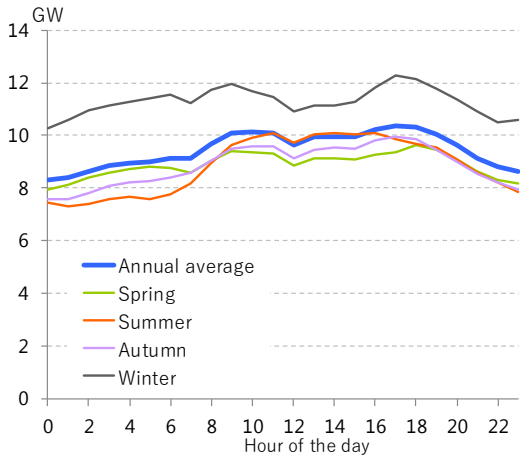

Tohoku

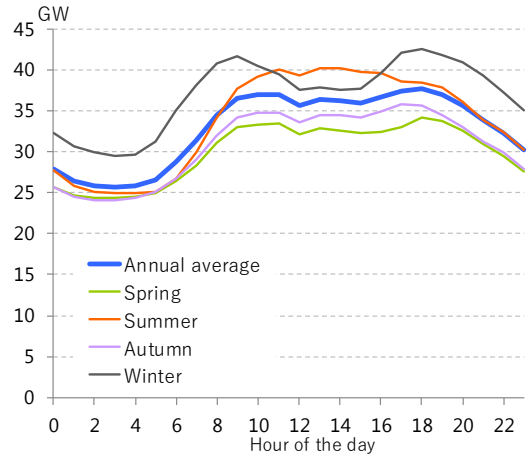

Tokyo

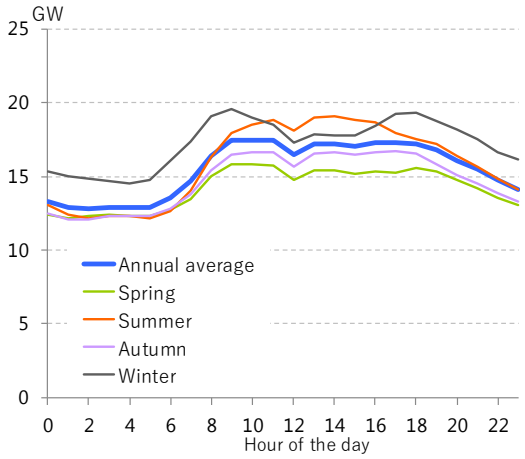

Chubu

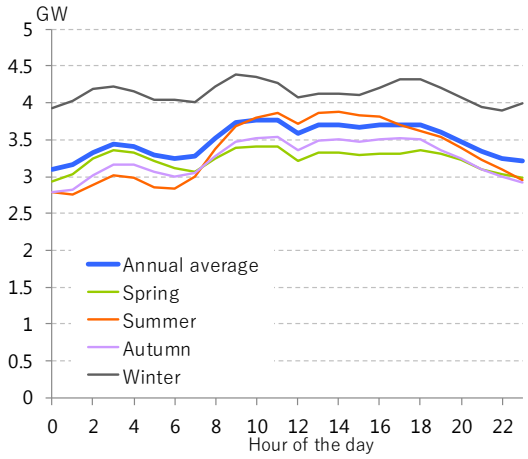

Hokuriku

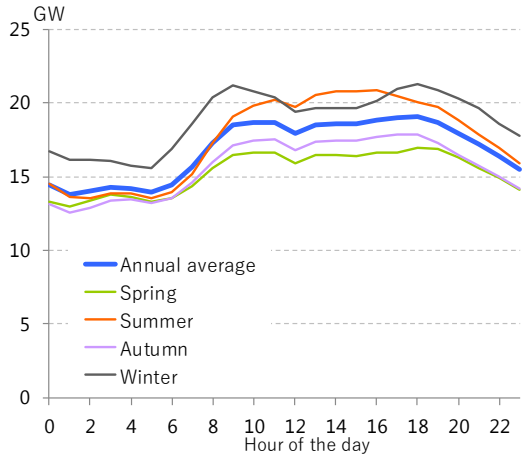

Kansai

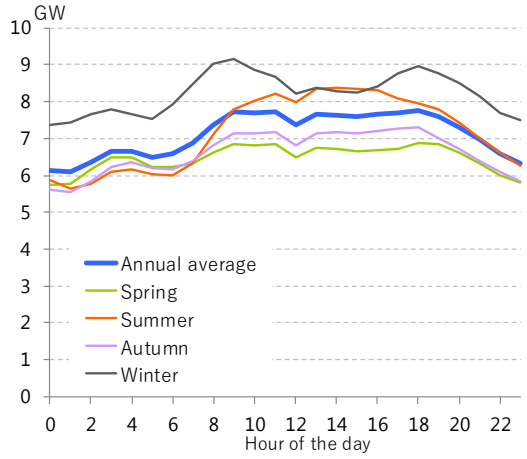

Chugoku

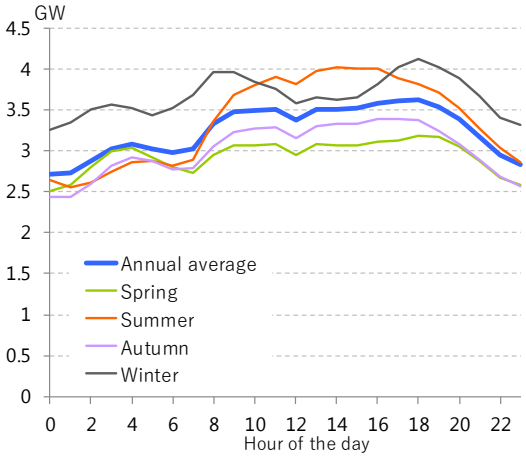

Shikoku

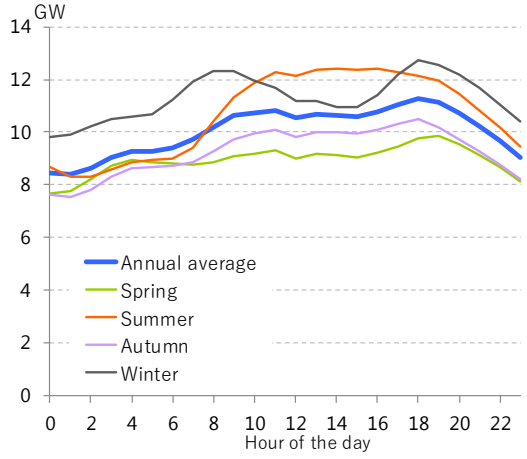

Kyushu

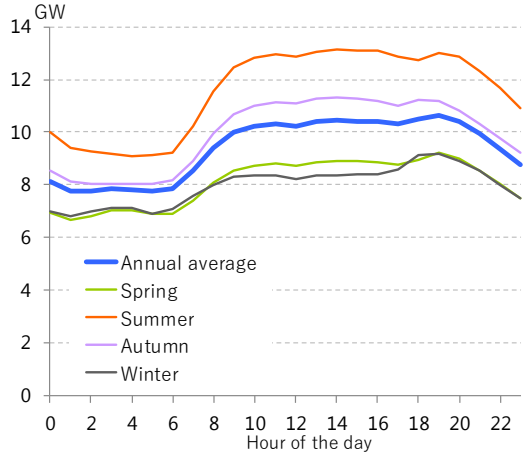

Okinawa

Sources: Websites of former general electric utilities

Figure A-3　Average daily load curve by area and season (Apr. 2017 – Mar. 2018)